New insights into the structural and functional involvement of the gate loop in AcrB export activity

Abdessamad Ababou[1,*]

[1] *University of East London, School of Health, Sport and Bioscience, Water Lane, London E15 4LZ, UK*

* Corresponding authors:

A. Ababou *email: a.ababou@uel.ac.uk. Tel: +44* 2082234589.

Abstract

AcrB is a major multidrug exporter in *Escherichia coli* and other Gram-negative bacteria. Its gate loop, located between the proximal and the distal pockets, have been reported to play important role in the export of many antibiotics. This loop location, rigidity and interactions with substrates have led recent reports to suggest that AcrB export mechanism operates in a sequential manner. First the substrate binds the proximal pocket in the access monomer, then it moves to bind the distal pocket in the binding monomer and subsequently it is extruded in the extrusion monomer. Recently, we have demonstrated that the gate loop is not required for the binding of Erythromycin but the integrity of this loop is important for an efficient export of this substrate. However, here we show that the antibiotic susceptibilities of the same AcrB gate loop mutants for Doxorubicin were unaffected, suggesting that this loop is not required for its export, and we demonstrate that this substrate may use principally the tunnel-1, located between transmembranes 8 and 9, more often than previously reported. To further explain our findings, here we address the gate loop mutations effects on AcrB solution energetics (fold, stability, molecular dynamics) and on the *in vivo* efflux of Erythromycin and Doxorubicin. Finally, we discuss the efflux and the discrepancy between the structural and the functional experiments for Erythromycin in these gate loop mutants.

Keywords

Bacterial multidrug resistance
AcrB-substrate interactions
AcrB export mechanism
X-ray crystallography
MD simulation

1. Introduction

AcrB is the principal efflux transporter in *E. coli*, located in the inner membrane of the bacteria, and plays an important role in capturing and expelling its substrates mainly from the periplasm [1-5]. AcrB has an extremely wide substrate specificity consisting of structurally diverse and unrelated compounds, including antibiotics, detergents, dyes, organic solvent, and biofuels [3, 6-10]. AcrB belongs to the superfamily of resistance nodulation and cell division (RND) transporters, and functions as a homotrimer where large conformational changes take place between the resting state, symmetric trimer in the absence of substrate, and the active state, asymmetric trimer in the presence of substrate [11-14].

Crystallographic studies of AcrB in complex with antibiotics have shown that these substrates bind either the proximal pocket in the access/loose monomer (access binding pocket) or the distal pocket in the binding/tight monomer (deep binding pocket) [11, 15, 16]. The observed binding of large substrates (Erythromycin (ERY) and Rifampicin) to the proximal pocket versus small substrates (Doxorubicin (DOX) and Minocyclin) binding to the distal pocket, and the presence of a loop (gate/switch loop), of ~ 10 amino acids, (**Fig. 1A**) separating these two main binding pockets have provided further insight into AcrB-substrate interactions and inspired the idea of a sequential or stepwise export mechanism for AcrB efflux activity [15, 16]. This implies the substrate binds the proximal pocket, then the distal pocket and subsequently to be extruded out of the cell via TolC. Such mechanism raises the question on the gate loop role and importance in this efflux mechanism, as it lies precisely between the proximal pocket and the distal pocket. In particular, the conformational change from the access monomer to the binding monomer results in an increased space within the distal pocket while a decreased space at the proximal pocket, and hence the gate loop may have direct implication toward substrates binding and export, as previously stated [15, 16].

Several reports have shown that mutation or deletion of residues at the gate loop affect AcrB export activity of several substrates to variable extent [15-20]. Crystallographic investigations of AcrB mutations at the gate loop, such as G616N and G616P-G619P, have been reported to indicate that this loop flexibility may play an important role in substrate transport during the undergoing conformational changes by the monomers between the access/loose, binding/tight, and extrusion/open states [15, 16]. In fact, it was reported that in G616N mutant the gate loop conformation in the access monomer resembles the one of the binding monomer in AcrB, and in G616P-G619P mutant the gate loop conformation in the binding monomer resembles the one of the access monomer in AcrB. This induced rigidity in these gate loop mutants was directly linked to the decrease in their antibiotics resistance [15, 16]. To rationalize the effect of

these gate loop mutations on AcrB substrates export, structural investigations at atomic resolution are crucial to underline the important interactions between these mutants and the substrates.

To understand the structural and functional importance of the gate loop in AcrB export activity, recently we have reported the structures of two mutants of this loop in the presence and absence of ERY; the triple mutant F615A-F617A-R620A (AAA), and the deletion mutant F615G-Δ[G616-R620] (ΔLoop), as they cover several of the reported mutations of the loop and making a large deletion of the loop, that has never been reported before. We have shown for the first time that this loop is not required structurally for the binding of ERY [21]. However, several aspects concerning the gate loop mutations effect on AcrB fold, stability and dynamics in solution, the trimeric state symmetry, the export of small substrate such as DOX, other explanations for the discrepancy between the structural and functional results for ERY, and further important structural details within these AcrB-ERY complexes were not addressed.

Consequently, in this work we will address several questions on the importance of the gate loop in the export of ERY and DOX, including its effect on AcrB (1) trimer symmetry, (2) solution fold and stability, (3) solution molecular dynamics, (4) antibiotics resistance, and (5) *in vivo* efflux. To address these questions, we have used X-ray crystallography to solve the structures of the mutants in the symmetrical trimer state, we have investigated AcrB and mutants fold and stability in solution using CD spectroscopy, we have used MD simulation to study AcrB and mutants molecular dynamics in solution, and we have performed their antibiotic susceptibility, minimum inhibitory concentration (MIC), and *in vivo* efflux assays.

2. Materials and Methods

2.1. Expression and purification of AcrB and mutants

WT AcrB plasmid, called pETHisAcrB, was used for the protein expression as previously described [22]. pETHisAcrB was used as template to produce our gate loop mutants, F615A-F617A-R620A (AAA), and F615G-Δ(G616-R620) (ΔLoop). Amino acids substitutions and deletion were achieved using 5′ phosphorylated primers, and standard mutagenesis protocols. Mutations were verified by sequencing the amplified mutant plasmids. To express WT AcrB and mutants *E. coli* cells lacking endogenous AcrB gene were used. Cells were grown at 30 ^{o}C in 2TY medium containing 50 mg/l carbenicillin to an OD600 of 0.6, when 0.5 mM IPTG was added for 4 h. Cells harvested by centrifugation were resuspended in 20 mM Tris pH 8.0, 500 mM NaCl, 5% glycerol, 2 mM $MgCl_2$. Cells were broken by 30k psi passage through a cell

disruptor. After centrifugation at 10,000xg for 10 min at 4 ^{o}C, the supernatant is centrifuged at 140,000xg for 1 h. The membrane pellet was resuspended and solubilised in 10 mM KPi pH 8.0, 100 mM NaCl, 10 mM imidazole and 1.0% n-dodecyl β-maltoside (DDM) for 1 h at 4 ^{o}C. Then the mixture was centrifuged for 1 h at 145,000xg and the supernatant was applied onto a Ni^{2+}-NTA agarose column pre-equilibrated with buffer A (20 mM KPi pH 8.0, 100 mM NaCl, 10 mM imidazole, 0.02% DDM). The column was washed with buffer B (20 mM KPi pH 8.0, 300 mM NaCl, 50 mM Imidazole, 0.02% DDM), and the proteins were eluted with buffer C (20 mM KPi pH 8.0, 100 mM NaCl, 300 mM Imidazole, 0.02% DDM). Proteins were buffer exchanged into 20 mM Tris pH 8.0, 100 mM NaCl, 0.1 or 0.03% DDM, using an Amicon 100 kDa molecular weight cut-off concentrator (Millipore).

2.2. Crystallization of AcrB and mutants

To search for initial hits, crystallization trials were carried out using several crystallization screening buffers, and using sitting drop over 96 well MRC plates (Molecular Dimensions) with the mixing of the protein solution and reservoir solution performed by Mosquito robot. Crystals were then manually optimized in 24 well plates. AcrB, AAA, and ΔLoop crystals were grown by the hanging drop vapour diffusion method at 15 ^{o}C, and at protein concentrations of 27, 24, and 20 mg/ml, respectively. The drops were made by mixing 2.0 μl of protein solution with 2.0 μl of crystallization solution, and equilibrated against 1 ml of the crystallization solution. The crystals were grown in buffer-1 (0.1 M ADA buffer at pH 7.4, 0.1 M Li_2SO_4, 10% PEG 3350), and were cryoprotected by stepwise addition of cryoprotectant as buffer-1 plus 22% glycerol or 25% ethylene glycol, before being flash-frozen in liquid nitrogen.

2.3. X-ray diffraction collection, structure phasing and refinement

X-ray diffraction data for screening and checking crystals quality were collected at Diamond Light Source (Didcot, UK). X-ray diffraction data were collected at 100 K on beamline PXIII at Swiss Light Source (SLS) at the Paul Scherrer Institut (Villigen PSI, Switzerland). X-ray data sets were indexed and integrated using iMosflm [23] and scaled using Scala or Aimless in the CCP4 suite [24]. The structures were solved by molecular replacement using Phaser [25] or Molrep [26]. Structures were solved using PDB file 3D9B [27] containing residues 1-1033. All Structures refinement were performed in two steps: First we used the recently reported refinement strategy combining the Rosetta sampling methodology and energy function with reciprocal-space X-ray refinement in Phenix [28], and then we continue the refinement using Phenix [29]. The structures were completed with iterative rounds of manual model-building with Coot [30] and refinement in Phenix. Figures were prepared using PyMol (www.pymol.org).

2.4. Circular dichroism spectroscopy and thermal unfolding

CD spectra were collected on an Aviv Model 410 CD spectrophotometer. Far-UV CD spectra were collected from 200 to 260 nm using a 1 mm cell path length and a 3 s averaging time. Thermal unfolding data were collected at 222 nm in the temperature range of 16 ^{o}C to 82 ^{o}C. Samples were placed in a 2 mm cuvette and heated in increments of 2 ^{o}C. All the experiments were carried out in 20 mM Tris pH 7.4, 100 mM NaCl, 0.03% DDM. The protein concentration was held constant at 5-10 μM. All CD measurements were corrected by subtracting the buffer spectra.

The unfolding experiments were fitted to a two-state model, and hence the CD unfolding data were fitted to

$$S = S_N + (S_U - S_N)/(1 + \exp(+\Delta G_{NU}/RT))$$

where S is the observed signal, and S_N and S_U are the CD signals for the unfolded and the native protein, respectively. ΔG_{NU} is the free energy difference of the unfolding reaction. Both the S_N and S_U were assumed to depend linearly on the temperature and the denaturant concentration, and to retain this linearity in the transition region.

For the thermal unfolding we assume that the heat capacity, ΔC_p^o, is temperature independent in the range of measurement [31], and hence the free energy of unfolding is

$$\Delta G_{NU}(T) = \Delta H_m + \Delta C_p^o\,(T - T_m) - T\,\{\Delta H_m/T_m + \Delta C_p^o \ln(T/T_m)\}$$

Where T_m is the melting temperature and ΔH_m is the enthalpy difference at T_m.

2.5. Antibiotic susceptibility and efflux assays

Single colonies of acrB deficient *E. coli* strain MC1061 harbouring AcrB and mutants, AAA and ΔLoop, plasmids were grown overnight at 37 ^{o}C in 2TY medium with 4μg/ml chloramphenicol and 25μg/ml carbenicillin. Bacteria growth was inoculated into 10 ml 2TY medium and grown at 37 ^{o}C to an OD at 600 nm of ~ 0.6-0.8, and then incubated for further ~ 30 min after adding 0.5 mM IPTG. Cells adjusted OD at 600 nm of ~ 0.06 were transferred to 100 μl 2TY medium containing 4μg/ml chloramphenicol and 25μg/ml carbenicillin, and ERY or DOX at 32 μg/ml and KAN at 4 μg/ml for the drug susceptibility test, and different concentrations after successive dilution of a starting concentration of ERY, DOX, and KAN of 2 mM, 1.14 mM and 2 mM,

respectively. The bacterial growth was measured using 96-well flat-bottomed plates (Nunc, Thermo Scientific), and a Synergy HTX Multi-Mode microplate reader (BioTek Instruments). After the overnight growth the drug susceptibility tests were plotted and the MIC's for ERY and DOX were determined. The experiments were performed in triplicate.

Similarly, for drug efflux assays we have grown cells at 37 ^{o}C to an OD at 600 nm of ~ 0.6-0.8, and then incubated for further ~ 30 min after adding 0.5 mM IPTG. The cells were then collected, washed twice with 100mM potassium phosphate buffer (pH 7.5 and containing 5mM $MgSO_4$) and then resuspended in the same buffer with an adjusted OD at 600 nm of 22. Each assay was performed in 96-well, flat-bottomed black plates (Nunc, Thermo Scientific) using a final cell volume of 100 ul, and doxorubicin (Sigma-Aldrich) was added to a final concentration of 29 μM, and for the competition assays, 29 μM ERY or KAN was added, as previously reported [16]. The fluorescence of DOX was measured using a Synergy HTX Multi-Mode microplate reader (BioTek Instruments) with an excitation wavelength of 485 nm and an emission wavelength of 620 nm. The fluorescence intensity decreased in a time-dependent manner owing to the accumulation of DOX in the cells, and the decrease in fluorescence intensity was prevented when DOX was expelled by an efflux pump. All the experiments were 3-4 times duplicated and the average data were plotted for the figures clarity.

2.6. Molecular dynamics simulation and trajectory analysis

Molecular dynamics simulations were performed using the AMBER package [32]. R32 crystal form structures of AcrB and mutants were used as starting structures. We performed our MD simulations using only the symmetric trimer structures of AcrB and mutants, as it is well accepted to be the resting state of the protein, where D407 and D408 are deprotonated. Consequently, if any structural effect that may occur due to the mutations will be better captured, and assessed in subsequent conformational changes of the proteins, than in an already functional state such as the asymmetric trimer where the protonation states of D407 and D408 should be taken into account [33]. The proteins were inserted in a pre-equilibrated 138 x 138 Å 1-palmitoyl-2-oleoyl-sn-glycero-3-phosphoethanolamine (POPE) membrane bilayer. AcrB's and mutants' central transmembrane cavity were manually filled by 13 POPE molecules. Clashes between POPE molecules and the proteins were removed. The AMBER force field parm99 was used for the protein and the TIP3P parameters for water [34], and GAFFlipid force field was used for POPE [35]. Standard protonation states were selected for all titratable residues. The proteins and POPE bilayer were submersed in a water box with Na+ ions to neutralize the system. The final simulation system for AcrB consisted of 90,344 atoms of the protein and POPE, 45 Na+ ions, 275,538 atoms of water, which make a total of 365,927

atoms. AAA simulation system consisted of 90,242 atoms of the protein and POPE, 48 Na+ ions, 275,559 atoms of water, which make a total of 365,849 atoms. ΔLoop simulation system consisted of 90,101 atoms of the protein and POPE, 48 Na+ ions, 275,559 atoms of water, which make a total of 365,708 atoms.

The time step was 2.0 fs with bonds fixed by SHAKE [36], the temperature was 300 K, van der Waals interactions were truncated at 10.0 Å, while electrostatic interactions were fully calculated with the Particle Mesh Ewald method [37]. After performing energy minimization only on the water molecules, the whole system was then energy minimized, and a 200 ps of solvent equilibrations at 300 K were calculated including the Na+ ions. Following equilibration, a trajectory of 10 ns was calculated for each molecular system. All the MD trajectories analysis, including the principal component analysis (PCA), was performed using AMBER package. Since the first three eigenvectors account for almost the total motions, we have projected our MD trajectories into the three-dimensional subspace defined by the top three principal components (X1, X2, and X3).

2. 7. Accession numbers

The atomic coordinates and structure factors of AcrB, AAA, and ΔLoop structures in space group R32 have been deposited to the Protein Data Bank with the accession code 4ZLJ, 4ZLL, 4ZLN, respectively.

3. Results

3.1. Structures of symmetric and asymmetric trimers of AcrB, AAA, and ΔLoop

Apo structures of AcrB and its gate loop mutants, AAA and ΔLoop, were solved in R32 space group for the symmetrical trimer as previously reported [27, 38, 39]. Detailed structures statistics are summarized in **Table S1**. Comparison of our structures in R32 space group with previously reported structures shows that our structures are consistent with symmetric form of AcrB (**Fig. 1B**), and have high structural similarities as reflected low RMSD's (< 1.05 Å) calculated on the whole main chain for each structure comparison (**Table S2**). The structures of AcrB and the mutants in R32 crystal form show that the gate loop mutations have no effect on the trimer state symmetry, as we recently reported for the asymmetric trimer of these mutants in $P2_1$ crystal form [21].

Previously we have reported the structures of AcrB and its gate loop mutants in $P2_1$ space group, in the presence and absence of ERY (**Fig. 1B**) [21], however several important structural details, involving the gate loop and thus their implication in the activity of AcrB, were not reported, in particular the detergent molecules binding and the ERY binding to the access monomer of the second trimer in our $P2_1$ structures. Details on Ni^{2+} presence and coordination are summarized in Supplementary Materials. Consequently, we will present and discuss these structural details in the following sections. Although there are similarities between our $P2_1$ form structures and the asymmetric trimer structures solved in P1 and C2 space groups, our structures present dissimilarities with their crystal packing [11, 12, 16]. For each trimer in our structures the presence of 5 trimers in close contact occurs, including direct contact between the docking domains, in a head to head configuration that has never been observed in other AcrB crystal packing (**Fig. S1**).

Importantly, comparison of the structures of AcrB and its mutants, AAA and ΔLoop, in either the apo form, in R32 and $P2_1$, or the complex form with ERY, in $P2_1$, revealed an overall highly conserved structures, and in particular in their export channel where the gate loop is located (**Fig. 1B,** and **Table S2**). This clearly shows that mutation or deletion of the gate loop, independently of the crystal forms, does not disrupt the overall fold, the trimer symmetry, and the 3D structure of AcrB.

3.2. Detergent binding to AcrB, AAA, and ΔLoop

In the AcrB and mutants structures we have solved previously in space group $P2_1$ [21], one detergent molecule (Dodecyl-β-D-maltoside, DDM, here called DDM-1) per monomer was found in the protein structures, in $P2_1$ form, in either the absence or presence of ERY (**Fig. 2A, 2B**, and **Fig. S3**). DDM-1 binding site consists predominately of residues S530, R536, R540, and Y541, and its binding revealed the presence of several potential hydrogen bonds (**Table S6, S7**). These observations suggest that DDM-1 has conserved binding mode. Interestingly, overlay of recently reported AcrB-AcrZ structure [40] with our structure monomers shows DDM-1 and AcrZ to share similar binding site with further similarities in their potential hydrogen bonds formation with residues S530, R536, R540, and Y541 (**Fig. 2**). Note that although the side chain of R536 is absent in AcrB-AcrZ structure, due to its close proximity to S37 in AcrZ strongly suggests that a hydrogen bond is highly possible to form between R536 and S37 (**Fig. 2E**). Consequently, taking into account the substantial specificity of DDM-1 binding, the sugar group in DDM-1 could be a potential lead fragment to block AcrB-AcrZ complex formation [41] and therefore to possibly disrupt the efflux pump activity, as suggested recently [42]. Remarkably, although we have used the exact same protein purification protocol and the

proteins samples have similar amount of DDM, no such DDM-1 binding has been observed in our R32 structures. This may suggest that either the crystal packing or the crystallization conditions may affect substantially the binding of DDM-1 molecules. Indeed, in $P2_1$ crystal form there is a hydrogen bond network formation between R536 and DDM-1 between AcrB monomers in crystal contact. This is absent in R32 crystal form as the nearest contact distance between monomers in crystal contact is between R536 and E962, however, a hydrogen bond between these donors and acceptors is ruled out as the nearest distance between is ~ 4.3 Å.

Surprisingly, in the presence of ERY the structures of AcrB and mutants revealed the presence of a second DDM molecule (DDM-2) binding only to monomer A and D within the groove formed by transmembrane 8 and 9 (TM8/TM9) (**Fig. 3,** and **Fig. S4**), which defines the entrance to tunnel-1 for AcrB substrates [11, 43]. While both trimers in our $P2_1$ crystal form are similar [21], strikingly the binding of DDM-2 in monomer A and D are substantially different (**Fig. 3B, 3C**). In monomer D, DDM-2 binds substantially higher in tunnel-1 as compared to its binding in monomer A, which resulted in different potential hydrogen bonds formation (**Table S7**). Comparison of our DDM-2 binding in our $P2_1$ structures with previously reported C2 structure with DDM-2 [15], shows highly conserved binding site for DDM-2 in either monomer A or D, nevertheless our DDM-2 in monomer D has clearly moved upward (**Fig. 3E, 3F**). Again, although we have used the exact same protein purification protocol and the proteins samples have similar amount of DDM, no such DDM-2 binding has been observed in our R32 structures. A rational explanation for this observation comes from the comparison of our R32 structure with $P2_1$ structure in the presence of ERY. Indeed, the DDM-2 molecule is in direct clash with the loop connecting the PC2 domain to TM8 in R32 structure, as shown in **Fig. 3G**, and also when compared with other R32 structures (**Fig. S5**).

Since the binding of DDM-2 have been reported by others in similar binding site and binding mode, it clearly substantiates the importance of this binding site for possibly other substrates of AcrB [15, 43], as we have shown for DDM-1 binding that mimics AcrZ binding to AcrB [40].

3.3. Substrate binding to AcrB, AAA, and ΔLoop

Although we succeeded to co-crystallize AcrB and its gate loop mutants with ERY and DOX in $P2_1$ space group, the X-ray diffraction data resulted in electron density maps that either have weak or merely no electron density to be assigned for either ERY or DOX around their reported binding sites or elsewhere in the structure [15, 16]. Similar situation has been reported for the binding of minocycline to AcrB mutant, G616N, at resolution of 2.9 Å [15]. Consequently, we have soaked the crystals, in P21 space group, of the proteins grown in the presence of ERY or

DOX in solution containing ERY or DOX. Subsequently, the X-ray diffraction data of the protein crystals in the presence of ERY revealed electron densities clearly identified for ERY in the proximal pocket [21]. Close inspection of the electron density maps elsewhere in the structure and in particular around A385-F386 loop revealed no possible electron density for bound ERY, as it was reported for the binding of linezolid to AcrB [44]. Unfortunately, with DOX we were unable to observe any plausible or realistic electron density for this substrate.

Structural comparison and analysis of ERY's binding to our AcrB, AAA, and ΔLoop structures and the reported AcrB-ERY structure [16], revealed high similarity in the binding mode of ERY in the proximal pocket (**Fig. 4**), as well as overall similar intermolecular interactions (**Table S8**). However, subtle but real differences were observed between ERY binding to the access monomers, A and D, in each trimer. Indeed, AcrB and mutants complex structures show ERY to superimpose well in monomer A as compared to monomer D (**Fig. 4**). Interestingly, such difference seems to correlate with the difference of DDM-2 binding to monomer A and D (**Fig. 3B, 3C**). Hence we speculate on the existence of some kind of influence between DDM-2 binding site and the proximal pocket where ERY binds, in particular when DDM-2 moved upward in the monomer D (**Fig. 3D**).

3.4. Antibiotics susceptibilities of AcrB, AAA, and ΔLoop

The surprising conserved binding of ERY to the mutants in our structures, and in particular with ΔLoop mutant, prompted us to investigate the *in vivo* involvement of the AcrB's gate loop using the antibiotic susceptibility and efflux transport for cells with AcrB and mutants genes. We have performed drug susceptibility test, drug efflux assay, and minimal inhibitory concentration (MIC) experiments for ERY, DOX for comparison as a smaller substrate, and Kanamycin (KAN) as a control since it is not a substrate of AcrB. Similar expression levels of AcrB and its gate loop variants were confirmed using western blot analysis (**Fig. S6**). In the absence of antibiotics, the cell growth of AcrB and mutants were similar to each other (**Fig. S7**). In the presence of ERY, at subinhibitory concentration of 32 μg/ml, the cell growth of the mutants were clearly affected and followed the decreasing order of AcrB > AAA > ΔLoop (**Fig. 5A**). However, at the same subinhibitory concentration of DOX the overall cell growth of AcrB and mutants were nearly similar, and in the presence of KAN, at subinhibitory concentration of 4 μg/ml, the cell growth of AcrB and mutants were similar (**Fig. 5A**). The MIC's results show the mutants to be highly susceptible to ERY when compared to AcrB, while the DOX susceptibility for AcrB and mutants were identical (**Table 1**).

To further investigate the gate loop effect on the AcrB substrates efflux, we have performed *in vivo* efflux of DOX, and ERY and KAN in the presence of DOX. The substrate efflux activity of AcrB and mutants was monitored by their ability to expel DOX that penetrated the cells. As shown in **Fig. 5B**, the control acrB-deficient cells (ΔacrB) accumulated DOX, as its fluorescence in the medium showed a time-dependent quenching. Instead the efflux of DOX by AcrB and mutants shows no fluorescence quenching, as DOX penetrating the cells was expelled to the medium (**Fig. 5B**). Similar result is observed for the efflux KAN by AcrB and mutants, where no substantial changes in DOX fluorescence took place, as expected since KAN is not a substrate of AcrB. Interestingly, the inhibition of DOX efflux (accumulation in the cells) in the presence of ERY shows similar DOX fluorescence quenching for AcrB, as previously reported [16], and mutants (**Fig. 5B**). While this implies the existence of efflux competition between DOX and ERY, it is worth noting that there is no substantial difference between AcrB and the mutants as observed for ERY susceptibility test (**Fig. 5A**).

These results strongly suggest that AcrB's gate loop is required for the well optimized and efficient export of ERY *in vivo*, while this loop is not required for the optimized DOX export.

3.5. Gate loop mutations effect on the solution fold and stability of AcrB

Taking into account the conflicting results between the structural and functional involvement of the gate loop in the export of ERY, we have addressed the effect of the gate loop mutations on the fold and stability of AcrB in solution, as such solution energetics may substantially affect AcrB export activity *in vivo* while undetected in the crystal structures analysis. Consequently, we have used CD spectroscopy to collect the far-UV CD spectra and the thermal unfolding data of AcrB and mutants, AAA and ΔLoop. The far-UV CD spectra of AcrB and mutants show no differences (**Fig. 6A**), suggesting that the mutants kept conserved secondary structures content and most probably overall similar structures to the WT in solution, as reported by our crystal structures (**Fig. 1**). The thermal denaturation results of the gate loop mutants revealed small shift in their melting curves as compared to the WT (**Fig. 6B**). A minor stability of the WT over the mutants is observed as shown by the Tm difference of ~ 3 ^{o}C (**Table 2**). However, such relatively small difference in Tm suggests an overall similar stability between the WT and the mutants, and in particular at physiological temperature (**Fig. 6B**). Hence, these results demonstrate that AcrB's gate loop mutations do not affect the fold and the overall stability of AcrB in solution, which is in good agreement with our reported X-ray structures of these mutants in either R32 or $P2_1$ crystal form [21].

3.6. Gate loop mutations effect on the molecular dynamics of AcrB

We performed MD simulations of AcrB and its gate loop mutants to assess the effect of these mutations on AcrB overall, intra- and inter-domains molecular dynamics. To assess the overall proteins conformational space sampling achieved during the MD simulations we performed principal component analysis (PCA) for the porter domain (PD) and the docking domain (DD) (**Fig. 1A**). The 3D plot of each monomer's PD/DD of each protein conformation, as projected into X1, X2 and X3 modes, shows a good conformational sampling amount by the proteins (**Fig. 7**). However, for better comparison between the proteins, 2D plots of X1/X2, X1/X3, and X2/X3 were carried out, and revealed the location of the starting conformations (**Fig. S8**). Although we have minimized our crystal structures and equilibrate the molecular systems prior to the MD trajectories calculations, these conformations were more often far from the conformation clusters sampled by the proteins (**Fig. S8**). This suggests that the proteins in solution may populate conformations that are slightly different to their crystal structures, as recently also reported for the asymmetric trimer of AcrB [45].

The RMSD's of the individual monomers with respect to their starting conformations were calculated, and nearly all the profiles show an overall similar trend in reaching a plateau, or nearly about as for 1 monomer in either AcrB or AAA, and being stable during the MD trajectories (**Fig. 8A**). Interestingly, for all proteins the RMSD profiles show two monomers to evolve nearly identically while the third monomer exhibits different behaviour. Strikingly, when we compare the calculated RMDS's between the monomers in the asymmetric trimer of AcrB similar observation occurs, namely RMSD(A/B), RMSD(A/C), and RMSD(B/C) were 1.96 Å, 3.24 Å, and 3.22 Å, respectively. The structural changes during the export activity of AcrB can be assessed by the conformational changes at PC1 (containing the gate loop) and PC2 domains within the monomers, which are involved in the AcrB functional rotating mechanism [11, 12]. Consequently, we have calculated the distance between PC1 and PC2 domains during our MD trajectories for AcrB and mutants (**Fig. 8B**). With the exception for monomer B of AAA and monomer C of ΔLoop, the overall trend in these distances were fairly similar for all the proteins. However, similar trend found in RMSD profiles (**Fig. 8A**) can also be observed here, as two monomers evolve nearly in similar way while the third monomer exhibits different behaviour (**Fig. 8B**), which is modest in AcrB while prominent in AAA and more stronger in ΔLoop.

The conformational changes that AcrB undergoes between symmetric to asymmetric trimer is well accepted to be directly linked to its export activity, due to the proton translocation at its transmembrane domain which plays a major role in such structural change [11-13]. In this work our structures were prepared for the MD simulations calculations with deprotonated D407 and

D408, which should lead to no conformational change, since the symmetric trimer is the resting state in the absence of ligand [46]. To check on the presence of any conformational change between the monomers in our proteins, we looked closely at the central small helix containing Q112, as in the extrusion monomer (monomer C in the asymmetric trimer) this helix is highly inclined when compared with the other monomers, where their helices are nearly perpendicular to the membrane plane. Hence, we calculated the angles between Q112 at each monomer using Cα atoms (**Fig. S9**). Surprisingly the calculated angles for the last 2 ns in all the proteins show one angle to be higher than the other two (**Table S9**), reporting similar trend as with the RMSD and PC1-PC2 distance profiles (**Fig. 8**). Interestingly, comparison of our angles with those of the asymmetric trimer revealed similar trend except for the other two angles, as they were slightly different to each other (**Table S9**). Our data clearly point to a tendency in the molecular dynamics behaviour of these symmetric trimers to somehow break from the strict symmetrical conformation. Beyond the implication of crystal packing forces, these molecular dynamics behaviour of AcrB and mutants, resulting in structural shift from the X-ray structures, suggest that the water motion within these proteins may play a role in such behaviour. Indeed, the water residency and movement were reported to play important role in the export mechanism of AcrB [47, 48].

Our AcrB and mutants in complex with ERY structures show that ERY binds specifically to the proximal pocket and in particular to K290 and S134 surrounded by S132-S135 (**Fig. 4, Table S8**). Hence to investigate the effect of the gate loop mutations on ERY binding site we calculated the RMSD's of the Serine-loop (S-Loop, S132-S135) (**Fig. S10**), and the hydration change at residues K290 and S134, using the radial distribution function (RDF) profiles providing the probability of finding water molecules at a given distance from the residue of interest. Overall similar RMSD's profiles are observed for the S-loop, with minor difference in monomer A (**Fig. S10B**). RDF profiles show an overall similar hydration of either S134 or K290, with small differences at distances above 4 Å, and the first hydration shell peak is centred around 2.8 Å for S134, while it is around 3.0 Å for K290 (**Fig. 8C-D, Fig S11**).

4. Discussion

Understanding how the efflux pump AcrAB-TolC works, and hence its contribution to the multidrug resistance in Gram-negative bacteria, necessitates a good understanding of the export mechanism of AcrB. This relies mainly on studying AcrB interactions with its substrates at atomic resolution. However, X-ray crystallography investigations of AcrB-substrate interactions has proven very challenging, since structures of AcrB with only five antibiotics (ERY, DOX, Minocycline, Rifampicin, and Puromycin), with the exception of an inhibitor ABI-PP

that shares similarities with the binding of DOX and Minocycline, and recent structures of the periplasmic part of AcrB in complex with MBX compounds and Rhodamine 6G, were reported [11, 15, 16, 49-51]. To further understand the AcrB export mechanism, we have investigated the role and the importance of the gate loop in AcrB interactions with ERY and DOX for their binding and *in vivo* export. In fact, several reports have shown that mutation or deletion of residues at the gate loop can affect AcrB export activity of several substrates to variable extent [16-19]. However, no direct structural evidence on the interaction of the substrates with these mutants has been reported prior to our work [21]. Consequently, we have characterized the mutations effect of the gate loop, AAA and ΔLoop, on AcrB's ERY binding, structure, trimer symmetry, solution fold, solution stability, molecular dynamics, and antibiotics resistance and efflux.

Our recent and present work results revealed unexpected findings on the role and importance of the gate loop in AcrB export mechanism. Indeed, it is unexpected to observe the binding of ERY to AAA and ΔLoop to be similar to the WT [21], while substantial increase in ERY susceptibility for the mutants was observed (**Fig. 5**, **Table 1**). Strikingly, despite the deletion of the gate loop in ΔLoop mutant, which results in further available space in the export channel to accommodate at least another ERY molecule in the access monomers (monomers A and D), and possibly the binding of ERY to the binding monomers (monomers B and E), the binding of ERY to the mutants is similar to its binding to the WT. This strongly suggests that ERY binds specifically to the proximal pocket in the access monomer. Interestingly, although ERY has to be translocated deeper beyond the proximal pocket, no alternative ERY binding site could be observed. In fact, we have predicted that ERY can bind favourably to the distal pocket using molecular docking and MD simulation (data not shown), as previously reported [52]. The multisite binding proximal and distal pockets of AcrB are large enough to physically accommodate more than one substrate, such as the possible binding of DOX and Minocyline in the distal pocket (see details in **Fig. S12**). However, although mutations in the distal pocket have been reported to dramatically increase the susceptibility of ERY [17], and the presence of several polar residues (S46, Q67, N68, N70, Q89, S128, E130, S167, D174, Q176) beyond the proximal pocket, which could provide alternative binding site(s) for ERY, our ΔLoop-ERY structure revealed no such possible binding sites for ERY. These observations suggest that beyond the proximal pocket, ERY's binding site, the translocation of ERY in the export channel of AcrB is possibly highly transient in nature, resulting in no stable AcrB-ERY interaction to be observed experimentally, at least in light of our findings [21]. This idea of highly transient binding of ERY is well strengthen by the recent proposed hypothesis of "multisite drug-oscillation" where the drug molecule oscillates between several drug binding sites in the large

binding pockets of AcrB (proximal and distal), and the suggestion that high molecular mass drugs, such as ERY, may be occluded without specific binding in the distal pocket [53].

Comparison with the reported structure of AcrB-ERY revealed structural differences at the gate loops around A618-R620 residues (**Fig. 4**) [16]. Overlay of AcrB and AAA structures in the presence of ERY shows the gate loop in AAA moved upward around A618 without affecting the binding of ERY, in particular in monomer A (**Fig. 4**). G616N and G616P-G619P mutations were reported to have increased the rigidity of the gate loop, in particular for G616P-G619P, which was claimed to explain their increased ERY and DOX susceptibilities [15, 16]. Our mutant, AAA cannot confer a rigid gate loop and hence the increase of ERY susceptibility for this mutant could not be explained by the rigidity of this loop. In fact, our MD simulations show the RMSD and RMSF of the gate loop in each monomer of AAA having higher structural variations and flexibility, respectively, than the WT loops, which is in line with rather flexible loop behaviour (**Fig. S13**). Furthermore, antibiotics resistance investigation of G616N reported that substrates with higher minimal projection areas, such as ERY, are less well transported than those with lower minimal projection areas due to the gate loop rigidity [20]. This may suggest that either the increase of the flexibility or the deletion of the gate loop should enhance the export of ERY. However, the triple alanine mutation and the deletion of this loop in AAA and ΔLoop mutants, respectively, show ERY to be less well exported in AAA and much less exported in ΔLoop (**Fig. 4, Table 2**). Hence, beyond how well ERY is exported when compared to other smaller substrates, the gate loop is somehow required for its well optimized export by AcrB. Indeed, either high or low flexibility of the gate loop resulted in less well exported ERY, which suggests that a well tuned and optimized flexibility, as present in the WT, is necessary to achieve better and well optimized export of ERY.

Interestingly, these gate loop mutations have no substantial effect on DOX transport (**Fig. 4, Table 2**), which suggests that DOX may use alternative translocation routes to the tunnel-2, where it has to interact with the gate loop as recently reported [15, 20]. Tunnel-1 where DDM-2 binds AcrB and mutants, in monomer A and D (**Fig. 3B, 3C**), has been suggested to be one of AcrB substrates' translocation routes [11, 43]. Indeed, L674W and A677W mutations were shown to reduce significantly DOX efflux activity, while nearly undetectable for S462K mutation [16]. In fact, mutations of AcrB were reported to substantially increase the export of biofuel molecules; in particular T678A mutation increased the export of α-pinene by 320% [10]. In addition, I63F and I671T mutations were reported to increase the susceptibility of several lower molecular weight drugs, which bind the distal pocket, while nearly unchanged susceptibility of many large AcrB substrates was observed [54]. These mutations are located nearby and above the sugar head group in DDM-2 molecule, as well as part of the tunnel-1 route toward the distal

pocket (**Fig. 3**). In addition, molecular docking and energy minimized AcrB structure with DOX in DDM2 binding site shows the binding similarity between these substrates, in particular at the sugar group part of DDM-2 (**Fig. S14**). Furthermore, the possibility that binding of DDM-2 may induce the subtle differences of ERY binding in monomer A and D (**Fig. 4**), suggests that tunnel-1 is indeed an active pathway for substrates such as detergent DDM and DOX. Hence, together these observations suggest that DOX may use both tunnel-1 and tunnel-2 as part of its translocation pathway [10, 15, 16, 20]. Nevertheless, the absence of any substantial effect of the gate loop mutations on the DOX export may be due to the combination of its translocation via tunnel-1 and its binding to the distal pocket overriding the binding of the proximal pocket as a result of the "multisite drug-oscillation" idea [53]. The above results and observations suggest that DDM-2 binding in tunnel-1, in monomer A and D, may be highly relevant for hydrophobic substrates having tunnel-1 as part of their translocation route, such as possibly detergent and DOX, as also recently suggested [53].

We have shown that the AcrB gate loop is not required for the binding of ERY (**Fig. 4**), while it is required for its well optimized export by AcrB (**Fig. 5, Table 1**). The efflux of ERY as indirectly measured by the fluorescence quenching of DOX, revealed similar efflux transport between AcrB and mutants (**Fig. 5B**). This shows that DOX efflux transport is decreased due to the competition with ERY, confirming that ERY and DOX use similar translocation pathway in AcrB export channel; at and beyond the distal pocket. Nevertheless, this result did not image the expected order of the observed increase of ERY susceptibility of the mutants (**Fig. 5A, Table 1**). Three explanations to this finding are possible; first, in the presence of ERY, DOX may principally use tunnel-1 instead of tunnel-2, used by ERY, to move toward the distal pocket without having to compete strongly with ERY and hence the observed ERY susceptibility of the mutants becomes virtually similar. Further evidence for this explanation, as explained above, was recently reported for AcrB I63F and I671T mutations [54], as well as previous reports on mutations such as L674W, A677W and S462K mutations [16] and T678A mutation [10], which are within the tunnel-1 route. Second, the lower molecular weight, size, and shape of DOX as compared to ERY may benefit DOX to translocate far easily and possibly faster than ERY as recently reported for other substrates [10, 20], which in turn may not be dramatically affected by the ERY susceptibility of the mutants resulting in virtually similar efflux of ERY by AcrB and mutants. Third, ERY export by the mutants maybe enhanced to a similar level by the presence of DOX and hence no difference is observed for DOX export, as recently reported for the strong increase of the efflux of nitrocefin in the presence of Arg β-naphthylamide [55]. Although, the mechanism by which this enhanced or stimulated export occurred is yet to be explained, in our case taking into account the large space within the distal pocket, which may accommodate for at least 2 substrates simultaneously (**Fig. S12**), and the transient nature of ERY binding to the

distal pocket may suggest that the binding of DOX to the distal pocket promotes the translocation of ERY toward its extrusion. This will result in ERY export to be similar for AcrB and the mutants.

Our structural data clearly show that AcrB gate loop (i) does not interfere with the binding of ERY (binding to the access monomer, to the proximal pocket, and with similar binding mode), and (ii) does not dictate the location of the binding site of ERY (proximal pocket versus distal pocket). This clearly suggests that the gate loop is not required for the binding of ERY. Also our mutants' structures reveal no effect on AcrB trimer symmetry, as their asymmetric and symmetric trimers were similar to the WT. Our solution energetics investigations show that the gate loop mutations did not affect the fold and the overall stability of the proteins. However, while the overall dynamics of AcrB and mutants may seem similar (RMSD, proximal binding site hydration), moderate to substantial effect was observed at their monomers intra-domain molecular dynamics (PC1 and PC2 domains, gate loop). In contrast, our functional results provide an opposite picture to the structural and solution energetics results (fold, stability), since the mutants showed an increase of their ERY susceptibility, which means that the gate loop is required for the well optimized export of ERY by AcrB. Furthermore, while reported structures of AcrB-DOX complexes exhibit the presence of 1 contact residue between the gate loop and DOX at F617 in the proximal pocket and at F615 in the distal pocket [11, 15], yet our results provide evidence that the gate loop is not required for the export of DOX. Consequently, this may highlight the flexibility between DOX translocation routes as it may use tunnel-1 and/or tunnel-2 depending on the availability of the route and/or the pressure of efficient transport by AcrB for the survival of the bacteria.

At this stage, it is not an easy task to provide an explanation, substantiated experimentally, able to reconcile our structural and functional results on the involvement of the gate loop in ERY export. However, an intuitive explanation to such discrepancy could be related to the binding affinities of ERY to AcrB and mutants. Indeed, our structures show that ERY binds the mutants similarly to AcrB, however we cannot quantify their binding affinities. Subsequently, If the binding affinity could be in decreasing order such as AcrB > AAA > ΔLoop, then this may seem to reflect the ERY resistance assay (**Fig. 5A**). However, it may be questionable to assume that the export of ERY will follow the same trend as the binding affinities and not the opposite order (AcrB < AAA < ΔLoop), when in general AcrB is highly efficient in exporting large number of unrelated and diverse substrates that may not bind specifically or tightly to its export channel. Instead, a plausible explanation for such link between the binding affinity and the export of ERY in these mutants may lie in the effect of these mutations on ERY binding oscillations (ERY oscillations between several binding sites) in the proximal pocket which in turn may affect its

translocation through the distal pocket [53]. This explanation also holds for DOX as it binds mainly the distal pocket and hence it is fair to suggest the binding affinities will be fairly similar resulting in similar export of DOX for AcrB and the mutants.

On the other hand, the emergence of this discrepancy between our structural and functional results, for ERY, suggests that beyond our knowledge of AcrB export mechanism, we have to consider the possibility that the structural binding of a substrate to AcrB and its translocation through the export channel *in vivo* may take place through multi-conformational states mechanism, where several of these conformational states are unknown in our *in vitro* structural studies, due to their transient nature and kinetics. Indeed, in *in vitro* we observe only the most stable conformational state within the final stage of this multi-conformational states mechanism as represented by the asymmetric trimer of AcrB. Consequently, while our mutants' structures show no overall difference with the WT, the conformational changes kinetics from the symmetric to the asymmetric trimer and beyond may hold the key to such discrepancy with our functional results. In fact, recent report has shown that AcrB mutation E673G increased ERY resistance 2 fold, while structurally no contact is detected between E673 and ERY [56]. Interestingly, while Q569R mutation has no effect on the resistance of ERY, as Q569 is located at the entrance to the proximal pocket (shortest contact ~ 10.0 Å), the double mutant Q569R-E673G showed also no change in ERY resistance [56]. Thus, such long range effect can only be associated with the effect of molecular dynamics which in turn may affect the conformational change kinetics in these mutants. Similar conclusion could be drawn for the double mutant I626R-E673G which decreased ERY resistance 8 fold while I626R alone decreased ERY resistance 4 fold [56]. In addition, in line with this explanation, deletion of 17 residues in the protruding loop of AcrB, which far from either proximal or distal pockets, resulted in high susceptibility for ERY with 32 fold lower MIC than WT, while the fold and stability of this AcrB mutant were unchanged [57]. Furthermore, our MD simulations show how mutation or deletion of the gate loop can affect the distance between PC1 and PC2 domains which are involved in the export channel structure of AcrB and the conformational change between access, binding and extrusion monomers during AcrB's functional rotation mechanism. This suggests that further in the export process time course such differences could affect the normal conformational change kinetics of AcrB, and hence resulting in different susceptibility for ERY in these gate loop mutants. Altogether these observations clearly strengthen the idea of the presence of conformational changes kinetics differences between these mutants leading to their ERY susceptibility differences.

5. Conclusion

In summary, our work shows that AcrB's gate loop is not required for the binding of ERY but required for its well optimized export by AcrB. However, this loop is not required for the export of DOX, suggesting that the possibility it may not be required for DOX binding since DOX mainly binds the distal pocket. We demonstrate that the gate loop flexibility did not enhance the export of ERY, which opposes recent report on the effect of rigidity of this loop on the export of this antibiotic. Based on our and previously reported experimental data, we show that DOX use tunnel-1 more often than tunnel-2 for its translocation route. To reconcile the discrepancy between our structural and functional results for ERY we have suggested two possible explanations; the mutations effect on ERY binding affinity and the conformational changes kinetics. Nevertheless, there are more experimental data, as presented here, along with observations from our molecular dynamics results, which favour the latter explanation.

Acknowledgements

We thank the beamline staff at the Diamond Light Source (Didcot, United Kingdom) and the Swiss Light Source (Villigen PSI – Switzerland) for their help. We thank the University of Cambridge and University of East London for their support for this work.

References

[1] S. Murakami, Multidrug efflux transporter, AcrB--the pumping mechanism, Curr Opin Struct Biol, 18 (2008) 459-465.
[2] H. Nikaido, Antibiotic resistance caused by gram-negative multidrug efflux pumps, Clin Infect Dis, 27 Suppl 1 (1998) S32-41.
[3] H. Nikaido, Y. Takatsuka, Mechanisms of RND multidrug efflux pumps, Biochim Biophys Acta, 1794 (2009) 769-781.
[4] K.M. Pos, Drug transport mechanism of the AcrB efflux pump, Biochim Biophys Acta, 1794 (2009) 782-793.
[5] X.Z. Li, H. Nikaido, Efflux-mediated drug resistance in bacteria, Drugs, 64 (2004) 159-204.
[6] H. Nikaido, Multidrug resistance in bacteria, Annu Rev Biochem, 78 (2009) 119-146.
[7] D. Ma, M. Alberti, C. Lynch, H. Nikaido, J.E. Hearst, The local repressor AcrR plays a modulating role in the regulation of acrAB genes of Escherichia coli by global stress signals, Mol Microbiol, 19 (1996) 101-112.
[8] D.G. White, J.D. Goldman, B. Demple, S.B. Levy, Role of the acrAB locus in organic solvent tolerance mediated by expression of marA, soxS, or robA in Escherichia coli, J Bacteriol, 179 (1997) 6122-6126.

[9] N. Tsukagoshi, R. Aono, Entry into and release of solvents by Escherichia coli in an organic-aqueous two-liquid-phase system and substrate specificity of the AcrAB-TolC solvent-extruding pump, J Bacteriol, 182 (2000) 4803-4810.
[10] J.L. Foo, S.S. Leong, Directed evolution of an E. coli inner membrane transporter for improved efflux of biofuel molecules, Biotechnol Biofuels, 6 (2013) 81.
[11] S. Murakami, R. Nakashima, E. Yamashita, T. Matsumoto, A. Yamaguchi, Crystal structures of a multidrug transporter reveal a functionally rotating mechanism, Nature, 443 (2006) 173-179.
[12] M.A. Seeger, A. Schiefner, T. Eicher, F. Verrey, K. Diederichs, K.M. Pos, Structural asymmetry of AcrB trimer suggests a peristaltic pump mechanism, Science, 313 (2006) 1295-1298.
[13] D.G. Thanassi, L.W. Cheng, H. Nikaido, Active efflux of bile salts by Escherichia coli, J Bacteriol, 179 (1997) 2512-2518.
[14] H. Nikaido, Structure and mechanism of RND-type multidrug efflux pumps, Adv Enzymol Relat Areas Mol Biol, 77 (2011) 1-60.
[15] T. Eicher, H.J. Cha, M.A. Seeger, L. Brandstatter, J. El-Delik, J.A. Bohnert, W.V. Kern, F. Verrey, M.G. Grutter, K. Diederichs, K.M. Pos, Transport of drugs by the multidrug transporter AcrB involves an access and a deep binding pocket that are separated by a switch-loop, Proc Natl Acad Sci U S A, 109 (2012) 5687-5692.
[16] R. Nakashima, K. Sakurai, S. Yamasaki, K. Nishino, A. Yamaguchi, Structures of the multidrug exporter AcrB reveal a proximal multisite drug-binding pocket, Nature, 480 (2011) 565-569.
[17] J.A. Bohnert, S. Schuster, M.A. Seeger, E. Fahnrich, K.M. Pos, W.V. Kern, Site-directed mutagenesis reveals putative substrate binding residues in the Escherichia coli RND efflux pump AcrB, J Bacteriol, 190 (2008) 8225-8229.
[18] W. Lu, M. Zhong, Q. Chai, Z. Wang, L. Yu, Y. Wei, Functional relevance of AcrB Trimerization in pump assembly and substrate binding, PLoS One, 9 (2014) e89143.
[19] C. Wehmeier, S. Schuster, E. Fahnrich, W.V. Kern, J.A. Bohnert, Site-directed mutagenesis reveals amino acid residues in the Escherichia coli RND efflux pump AcrB that confer macrolide resistance, Antimicrob Agents Chemother, 53 (2009) 329-330.
[20] H.J. Cha, R.T. Muller, K.M. Pos, Switch-loop flexibility affects transport of large drugs by the promiscuous AcrB multidrug efflux transporter, Antimicrob Agents Chemother, 58 (2014) 4767-4772.
[21] A. Ababou, V. Koronakis, Structures of Gate Loop Variants of the AcrB Drug Efflux Pump Bound by Erythromycin Substrate, PLoS One, 11 (2016) e0159154.

[22] T. Touze, J. Eswaran, E. Bokma, E. Koronakis, C. Hughes, V. Koronakis, Interactions underlying assembly of the Escherichia coli AcrAB-TolC multidrug efflux system, Mol Microbiol, 53 (2004) 697-706.
[23] T.G. Battye, L. Kontogiannis, O. Johnson, H.R. Powell, A.G. Leslie, iMOSFLM: a new graphical interface for diffraction-image processing with MOSFLM, Acta Crystallogr D Biol Crystallogr, 67 (2011) 271-281.
[24] M.D. Winn, C.C. Ballard, K.D. Cowtan, E.J. Dodson, P. Emsley, P.R. Evans, R.M. Keegan, E.B. Krissinel, A.G. Leslie, A. McCoy, S.J. McNicholas, G.N. Murshudov, N.S. Pannu, E.A. Potterton, H.R. Powell, R.J. Read, A. Vagin, K.S. Wilson, Overview of the CCP4 suite and current developments, Acta Crystallogr D Biol Crystallogr, 67 (2011) 235-242.
[25] A.J. McCoy, R.W. Grosse-Kunstleve, P.D. Adams, M.D. Winn, L.C. Storoni, R.J. Read, Phaser crystallographic software, J Appl Crystallogr, 40 (2007) 658-674.
[26] A. Vagin, A. Teplyakov, Molecular replacement with MOLREP, Acta Crystallogr D Biol Crystallogr, 66 (2010) 22-25.
[27] D. Veesler, S. Blangy, C. Cambillau, G. Sciara, There is a baby in the bath water: AcrB contamination is a major problem in membrane-protein crystallization, Acta Crystallogr Sect F Struct Biol Cryst Commun, 64 (2008) 880-885.
[28] F. DiMaio, N. Echols, J.J. Headd, T.C. Terwilliger, P.D. Adams, D. Baker, Improved low-resolution crystallographic refinement with Phenix and Rosetta, Nat Methods, 10 (2013) 1102-1104.
[29] P.D. Adams, P.V. Afonine, G. Bunkoczi, V.B. Chen, I.W. Davis, N. Echols, J.J. Headd, L.W. Hung, G.J. Kapral, R.W. Grosse-Kunstleve, A.J. McCoy, N.W. Moriarty, R. Oeffner, R.J. Read, D.C. Richardson, J.S. Richardson, T.C. Terwilliger, P.H. Zwart, PHENIX: a comprehensive Python-based system for macromolecular structure solution, Acta Crystallogr D Biol Crystallogr, 66 (2010) 213-221.
[30] P. Emsley, B. Lohkamp, W.G. Scott, K. Cowtan, Features and development of Coot, Acta Crystallogr D Biol Crystallogr, 66 (2010) 486-501.
[31] P.L. Privalov, Stability of proteins: small globular proteins, Adv Protein Chem, 33 (1979) 167-241.
[32] D.A. Case, T.A. Darden, T.E. Cheatham III, C.L. Simmerling, J. Wang, R.E. Duke, R. Luo, R.C. Walker, W. Zhang, K.M. Merz, B. Roberts, B. Wang, S. Hayik, A. Roitberg, G. Seabra, I. Kolossváry, K.F. Wong, F. Paesani, J. Vanicek, J. Liu, X. Wu, S.R. Brozell, T. Steinbrecher, H. Gohlke, Q. Cai, X. Ye, J. Wang, M.-J. Hsieh, G. Cui, D.R. Roe, D.H. Mathews, M.G. Seetin, C. Sagui, V. Babin, T. Luchko, S. Gusarov, A. Kovalenko, P.A. Kollman, AMBER 11, University of California, San Francisco, (2010).

[33] M.A. Seeger, K. Diederichs, T. Eicher, L. Brandstatter, A. Schiefner, F. Verrey, K.M. Pos, The AcrB efflux pump: conformational cycling and peristalsis lead to multidrug resistance, Curr Drug Targets, 9 (2008) 729-749.
[34] W.L. Jorgensen, J. Chandrasekhar, J.D. Madura, M.L. Klein, Comparison of simple potential functions for simulating liquid water, J Chem Phys, 79 (1983) 926–935.
[35] C.J. Dickson, L. Rosso, R.M. Betz, R.C. Walker, I.R. Gould, GAFFlipid: a General Amber Force Field for the accurate molecular dynamics simulation of phospholipid Soft Matter, 8 (2012) 9617-9627.
[36] J. Ryckaert, G. Ciccotti, H. Berendsen, Numerical integration of the Cartesian equations of motion for a system with constraints: molecular dynamics of n-alkanes, J Comput Phys, 23 (1977) 327–341.
[37] T.A. Darden, D. York, L. Pedersen, Particle Mesh Ewald: an N log(N) method for Ewald sums in large systems, J Chem Phys, 98 (1993) 10089-.
[38] D. Das, Q.S. Xu, J.Y. Lee, I. Ankoudinova, C. Huang, Y. Lou, A. DeGiovanni, R. Kim, S.H. Kim, Crystal structure of the multidrug efflux transporter AcrB at 3.1A resolution reveals the N-terminal region with conserved amino acids, J Struct Biol, 158 (2007) 494-502.
[39] S. Murakami, R. Nakashima, E. Yamashita, A. Yamaguchi, Crystal structure of bacterial multidrug efflux transporter AcrB, Nature, 419 (2002) 587-593.
[40] D. Du, Z. Wang, N.R. James, J.E. Voss, E. Klimont, T. Ohene-Agyei, H. Venter, W. Chiu, B.F. Luisi, Structure of the AcrAB-TolC multidrug efflux pump, Nature, 509 (2014) 512-515.
[41] E.C. Hobbs, X. Yin, B.J. Paul, J.L. Astarita, G. Storz, Conserved small protein associates with the multidrug efflux pump AcrB and differentially affects antibiotic resistance, Proc Natl Acad Sci U S A, 109 (2012) 16696-16701.
[42] H. Venter, R. Mowla, T. Ohene-Agyei, S. Ma, RND-type drug efflux pumps from Gram-negative bacteria: molecular mechanism and inhibition, Front. Microbiol., 6 (2015).
[43] G. Sennhauser, P. Amstutz, C. Briand, O. Storchenegger, M.G. Grutter, Drug export pathway of multidrug exporter AcrB revealed by DARPin inhibitors, PLoS Biol, 5 (2007) e7.
[44] L.W. Hung, H.B. Kim, S. Murakami, G. Gupta, C.Y. Kim, T.C. Terwilliger, Crystal structure of AcrB complexed with linezolid at 3.5 A resolution, J Struct Funct Genomics, 14 (2013) 71-75.
[45] N. Fischer, C. Kandt, Porter domain opening and closing motions in the multi-drug efflux transporter AcrB, Biochim Biophys Acta, 1828 (2013) 632-641.
[46] C.C. Su, M. Li, R. Gu, Y. Takatsuka, G. McDermott, H. Nikaido, E.W. Yu, Conformation of the AcrB multidrug efflux pump in mutants of the putative proton relay pathway, J Bacteriol, 188 (2006) 7290-7296.
[47] N. Fischer, C. Kandt, Three ways in, one way out: water dynamics in the trans-membrane domains of the inner membrane translocase AcrB, Proteins, 79 (2011) 2871-2885.

[48] R. Schulz, A.V. Vargiu, P. Ruggerone, U. Kleinekathofer, Role of water during the extrusion of substrates by the efflux transporter AcrB, J Phys Chem B, 115 (2011) 8278-8287.
[49] R. Nakashima, K. Sakurai, S. Yamasaki, K. Hayashi, C. Nagata, K. Hoshino, Y. Onodera, K. Nishino, A. Yamaguchi, Structural basis for the inhibition of bacterial multidrug exporters, Nature, 500 (2013) 102-106.
[50] H. Sjuts, A.V. Vargiu, S.M. Kwasny, S.T. Nguyen, H.S. Kim, X. Ding, A.R. Ornik, P. Ruggerone, T.L. Bowlin, H. Nikaido, K.M. Pos, T.J. Opperman, Molecular basis for inhibition of AcrB multidrug efflux pump by novel and powerful pyranopyridine derivatives, Proc Natl Acad Sci U S A, (2016).
[51] Z. Wang, G. Fan, C.F. Hryc, J.N. Blaza, Serysheva, II, M.F. Schmid, W. Chiu, B.F. Luisi, D. Du, An allosteric transport mechanism for the AcrAB-TolC multidrug efflux pump, Elife, 6 (2017).
[52] A.V. Vargiu, H. Nikaido, Multidrug binding properties of the AcrB efflux pump characterized by molecular dynamics simulations, Proc Natl Acad Sci U S A, 109 (2012) 20637-20642.
[53] A. Yamaguchi, R. Nakashima, K. Sakurai, Structural basis of RND-type multidrug exporters, Front Microbiol, 6 (2015) 327.
[54] S. Schuster, M. Vavra, W.V. Kern, Evidence of a Substrate-Discriminating Entrance Channel in the Lower Porter Domain of the Multidrug Resistance Efflux Pump AcrB, Antimicrob Agents Chemother, 60 (2016) 4315-4323.
[55] A.D. Kinana, A.V. Vargiu, H. Nikaido, Some ligands enhance the efflux of other ligands by the Escherichia coli multidrug pump AcrB, Biochemistry, 52 (2013) 8342-8351.
[56] N. Kobayashi, N. Tamura, H.W. van Veen, A. Yamaguchi, S. Murakami, beta-Lactam selectivity of multidrug transporters AcrB and AcrD resides in the proximal binding pocket, J Biol Chem, 289 (2014) 10680-10690.
[57] W. Lu, M. Zhong, Y. Wei, Folding of AcrB Subunit Precedes Trimerization, J Mol Biol, 411 (2011) 264-274.

Figure Legends:

Fig. 1. Crystal structure of AcrB and gate loop mutants. (A) AcrB monomer depicting the docking domain (DD), the porter domain (PD), the transmembrane domain (TMD) and a close up view of the gate loop. (B) Structural comparison between AcrB (green) and its mutants, AAA (magenta) and ΔLoop (blue), in R32 (symmetric trimer, PDB: 4ZLJ, 4ZLL, 4ZLN) and $P2_1$ (asymmetric trimer) space groups. For the structures in $P2_1$ in the absence (- ERY) (PDB: 4ZIT, 4ZIV, 4ZIW) or presence (+ ERY) (PDB: 4ZJL, 4ZJO, 4ZJQ) of ERY, and for clarity ERY molecules are not shown. Top figure is the superposition of the overall structures (only access monomer A for $P2_1$ structures), and bottom figure is a close-up view at the export channel (proximal pocket, gate loop, and distal pocket), depicting the overall structural conservation.

Fig. 2. Binding of DDM-1 molecule to AcrB, AAA, and ΔLoop in $P2_1$. (A) AcrB access monomer, in the absence of ERY, exhibiting the location of DDM-1 molecule (yellow sticks). (B) 2Fo – Fc electron density map of DDM-1 binding to monomer A (access monomer in trimer-1) and contoured at 1.0 σ. (C) Overlay of our AcrB and reported AcrB-AcrZ structures and depicting the overlap between DDM-1 and part of AcrZ (L28-S37). (D) Binding site of DDM-1 and its potential hydrogen bonds. (E) Binding of AcrZ at DDM-1 binding site, including the potential hydrogen bonds.

Fig. 3. Binding of DDM-2 molecule to AcrB, AAA, and ΔLoop in $P2_1$. (A) AcrB access monomer, in the presence of ERY (green sticks), exhibiting the location of DDM-1 and DDM-2 molecules (yellow sticks). (B) 2Fo – Fc electron density map of DDM-2 binding to monomer A (access monomer in trimer-1) and contoured at 1.0 σ. (C) 2Fo – Fc electron density map of DDM-2 binding to monomer D (access monomer in trimer-2) and contoured at 1.0 σ. (D) Close-up view of ERY and DDM-2 in their binding site in tunnel 2 and 1, respectively. (E) Overlay of the monomer A and the access monomer from AcrB structure 4DX5 (orange and DDM-2 in blue), showing the similarities between DDM-2 molecules. (F) Overlay of the monomer D and the access monomer from AcrB structure 4DX5 (orange and DDM-2 in blue), showing the binding position shift of our DDM-2 molecule. (G) Overlay of the monomer A and our AcrB structure in R32 form.

Fig. 4. Binding of ERY to AcrB, AAA, and ΔLoop in the access monomer A (Trimer-1) and D (Trimer-2). Structures overlay of the access monomer with a close up view at the binding site of ERY and the corresponding gate loop in AcrB (green), AAA (magenta), ΔLoop (blue), and the reported structure of AcrB-ERY (pdb code 3AOC, yellow).

Fig. 5. Antibiotic susceptibility test and efflux assay for AcrB and its gate loop mutants, including the control ΔacrB (cells lacking acrB gene). (A) Antibiotic susceptibility test of ERY, DOX, and KAN at subinhibitory concentrations. (B) DOX efflux and competitive inhibition of DOX efflux by ERY and KAN, as monitored by DOX fluorescence quenching.

Fig. 6. Solution fold and stability of AcrB, AAA, and ΔLoop. (A) Far-UV CD spectra. (B) Thermal denaturation plot of the apparent fraction of unfolded protein (Fapp) as a function of temperature.

Fig. 7. Principal component analysis (PCA) of the porter domain and the docking domain of AcrB, AAA and ΔLoop. The first three principal modes were included in the present study to analyze the states of the monomers A (black), B (blue) and C (red). Each data point represents a different conformation of the monomers.

Fig. 8. Effect of the gate loop mutations on the molecular dynamics of AcrB and ERY binding site hydration. (A) Proteins stability as assessed by calculated RMSD's over the Cα atoms. (B) Distance changes between PC1 and PC2 domains as calculated between their centroid using the Cα atoms. (C) S134 backbone oxygen to water oxygen radial distribution function. (D) K292 side chain nitrogen to water oxygen radial distribution function.

Table

Table 1. Antibiotics susceptibilities of AcrB, AAA, and ΔLoop (MIC in μg/ml)

Antibiotic	ΔacrB	AcrB	AAA	ΔLoop
ERY	23	367	92	46
DOX	10	331	331	331
KAN	9	5	5	18

Table 2. Thermal unfolding parameters

Protein	ΔC_p (kcal/mol . K)[a]	ΔH_m (kcal/mol)[a]	T_m (^oC)	ΔT_m (^oC)
AcrB	-3.69	90.12	55.0	---
AAA	-4.82	98.91	51.7	**3.3**
ΔLoop	-3.51	88.94	51.5	**3.5**

[a] These parameters are reported for completeness

Figure

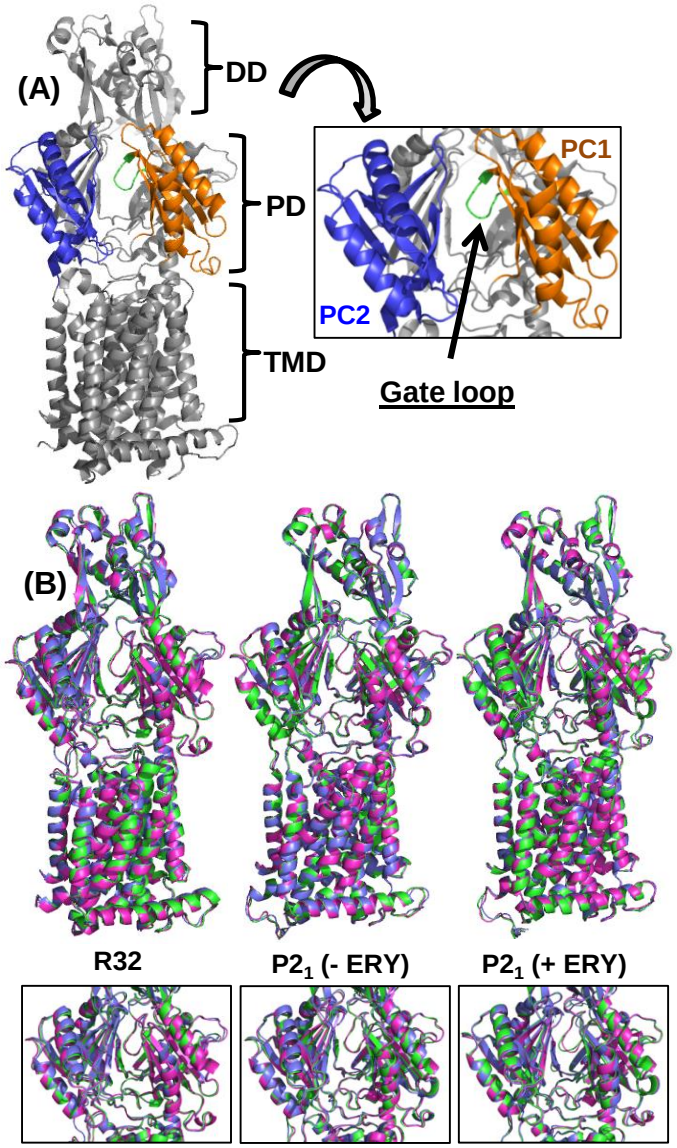

Fig. 1

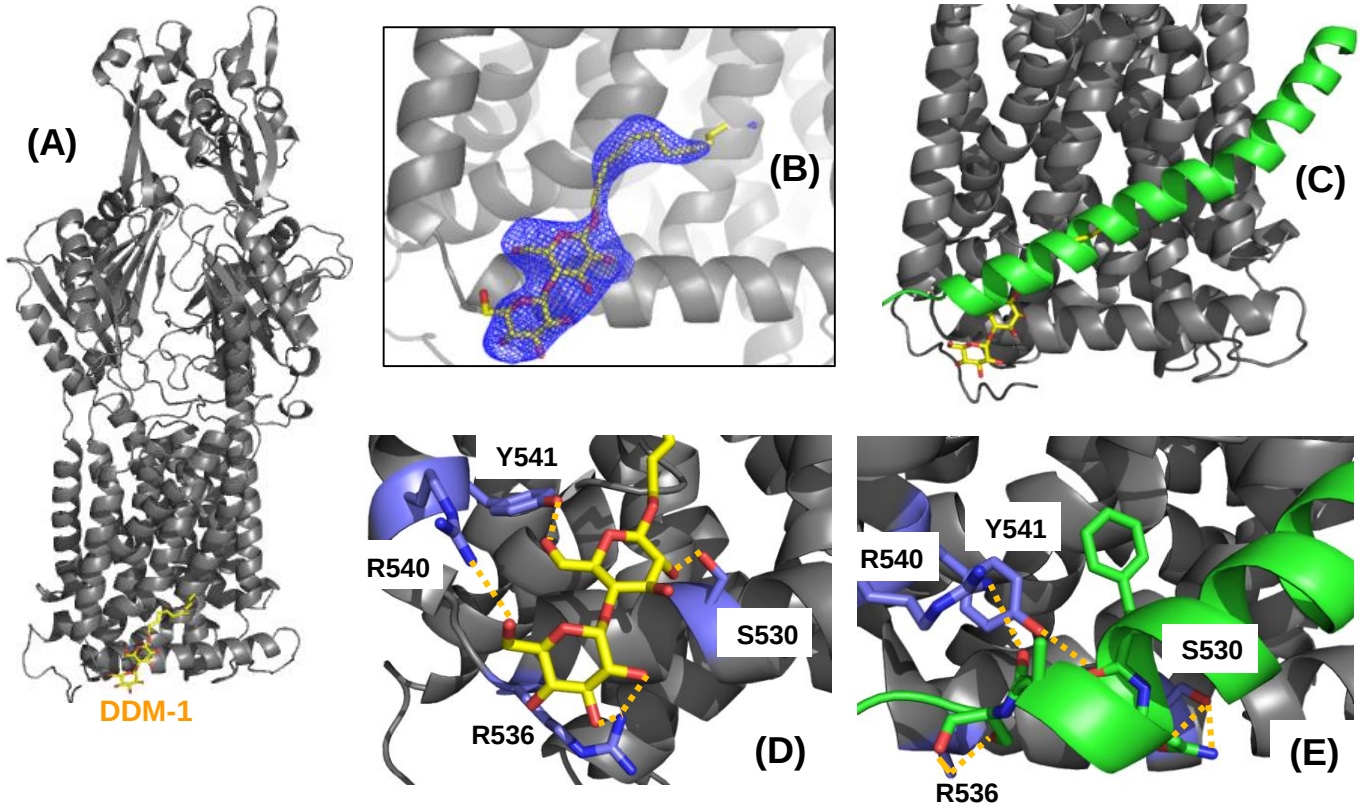

Fig. 2

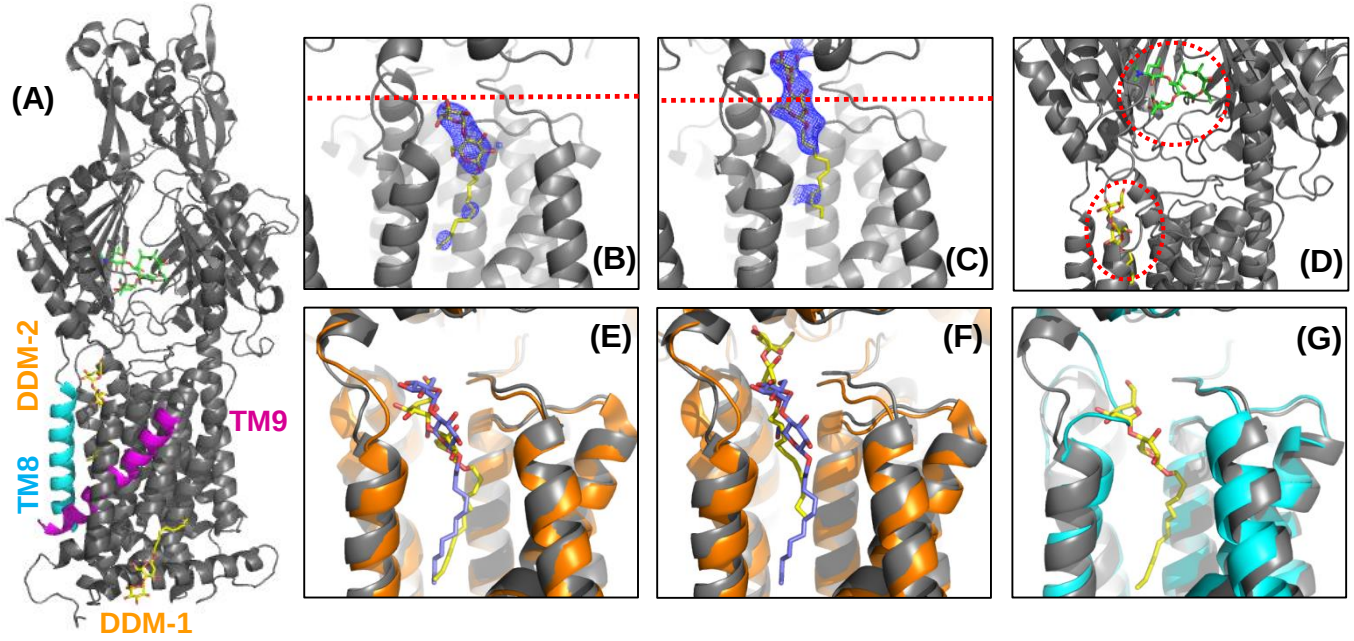

Fig. 3

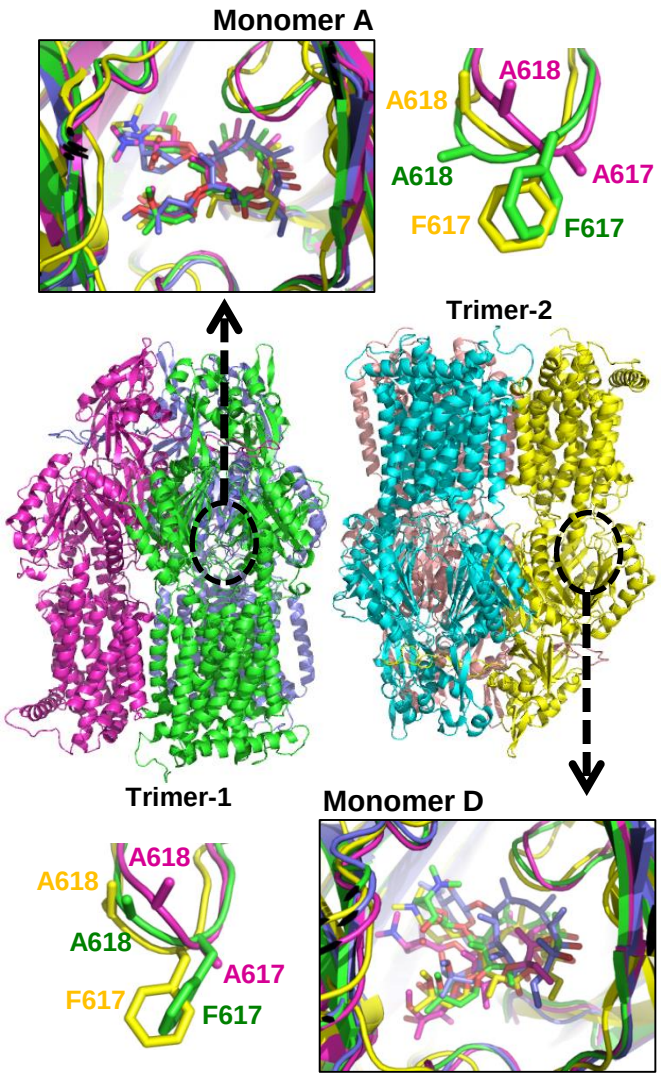
Monomer A
A618
A618
A618
A617
F617
F617
Trimer-2
Trimer-1
Monomer D
A618
A618
A618
A617
F617
F617

Fig. 4

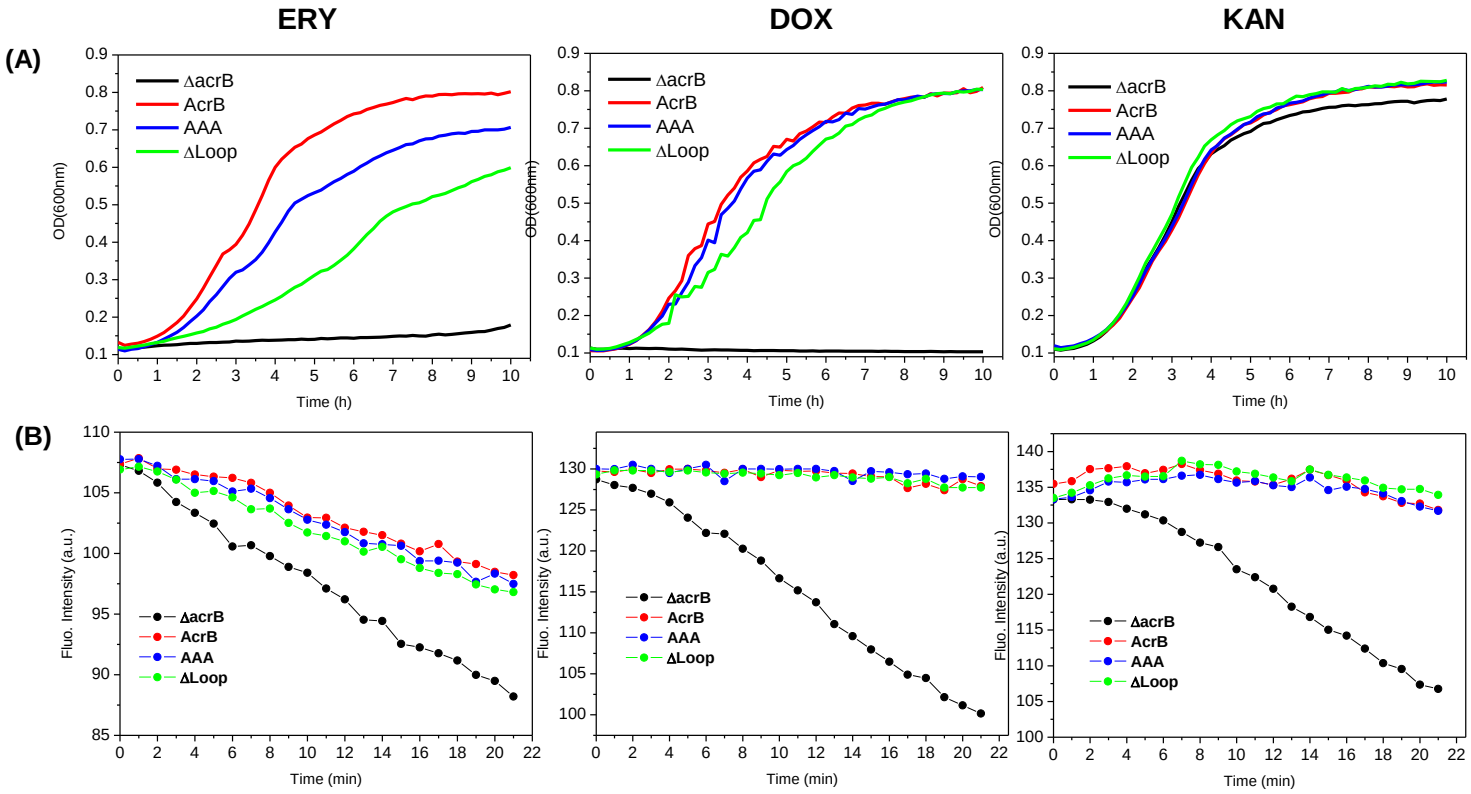
ERY
DOX
KAN
(A)
(B)
ΔacrB
AcrB
AAA
ΔLoop
OD(600nm)
Time (h)
Fluo. Intensity (a.u.)
Time (min)

Fig. 5

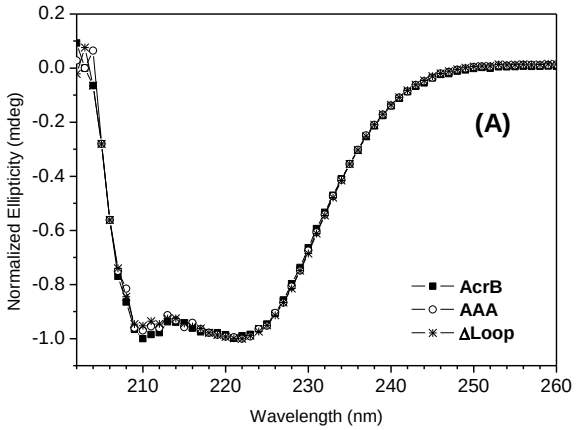
0.2
0.0
-0.2
-0.4
-0.6
-0.8
-1.0
Normalized Ellipticity (mdeg)
(A)
AcrB
AAA
ΔLoop
210
220
230
240
250
260
Wavelength (nm)

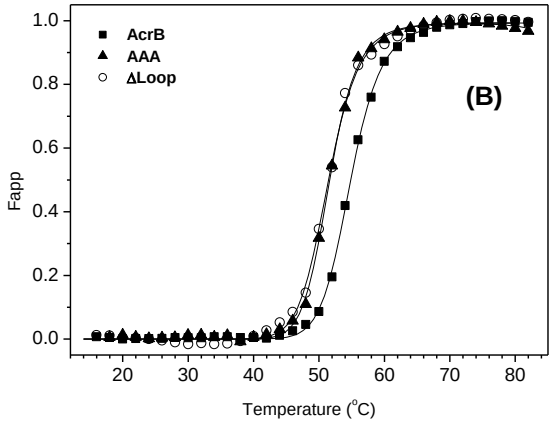
1.0
0.8
0.6
0.4
0.2
0.0
Fapp
AcrB
AAA
ΔLoop
(B)
20
30
40
50
60
70
80
Temperature (°C)

Fig. 6

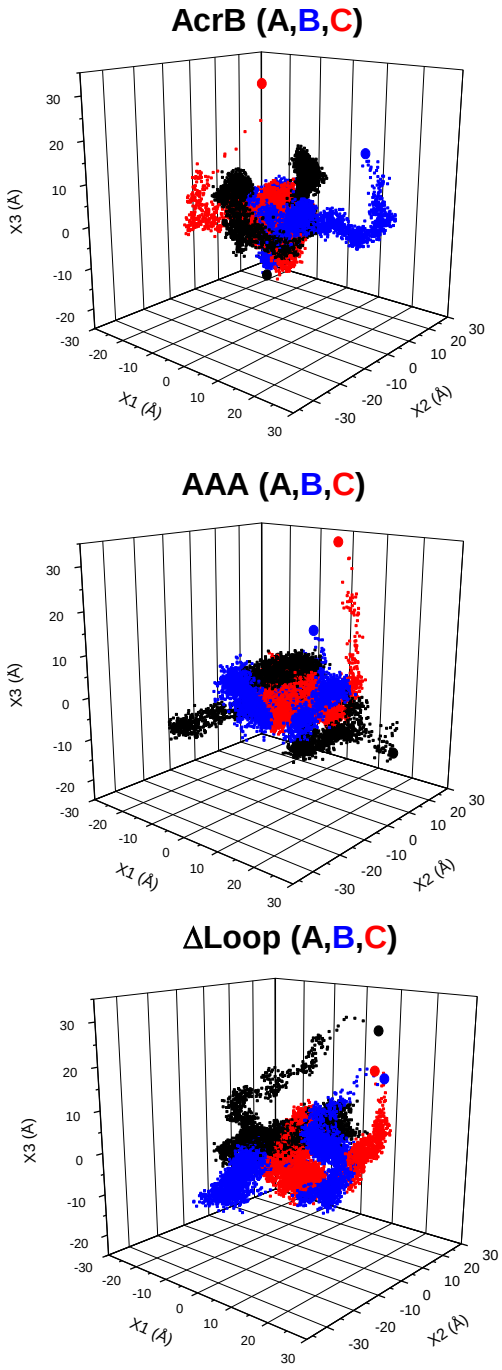

Fig. 7

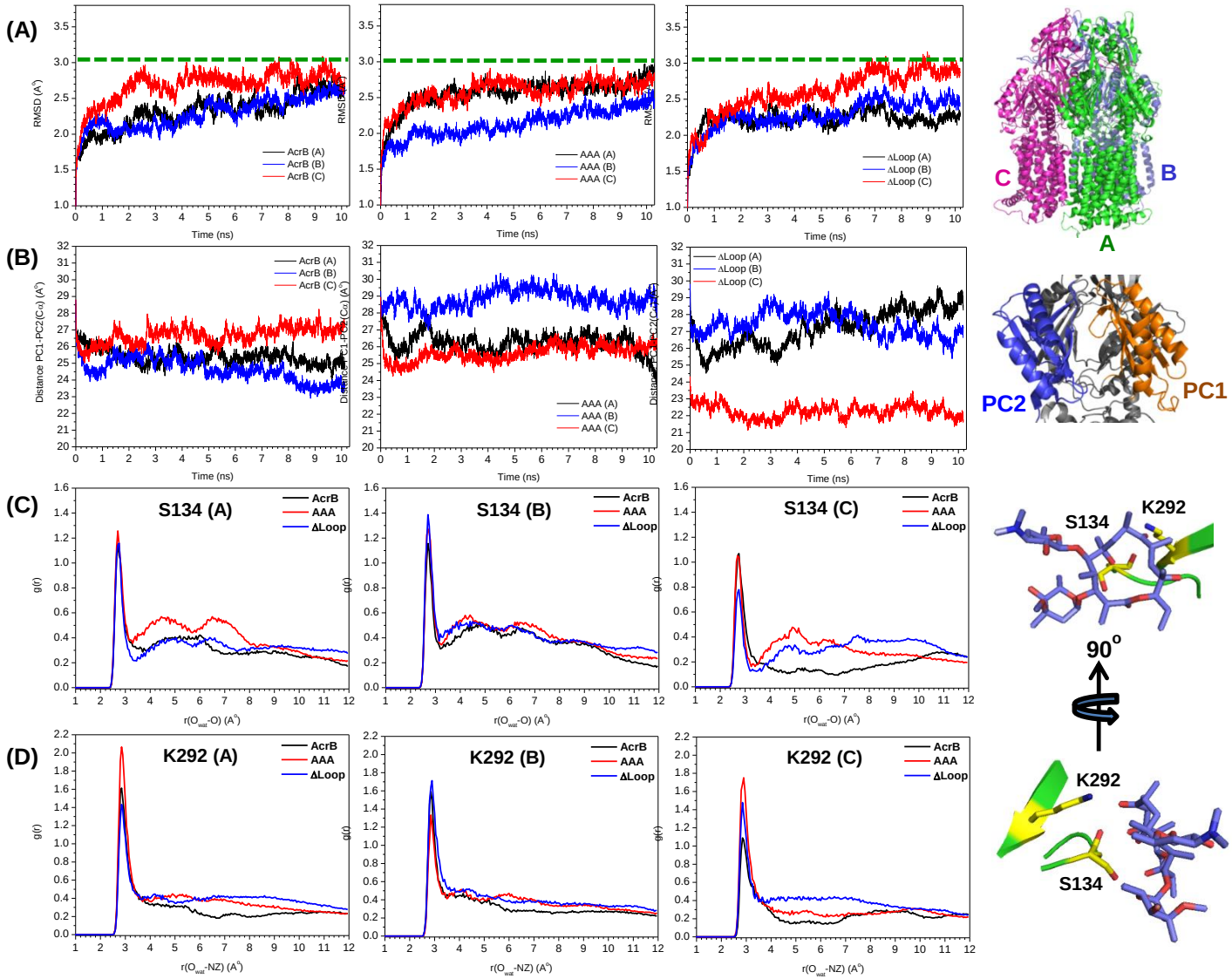
(A)
RMSD (A°)
Time (ns)
AcrB (A)
AcrB (B)
AcrB (C)
AAA (A)
AAA (B)
AAA (C)
ΔLoop (A)
ΔLoop (B)
ΔLoop (C)
C
B
A
(B)
Distance PC1-PC2(Cα) (A°)
PC1
PC2
(C)
S134 (A)
S134 (B)
S134 (C)
AcrB
AAA
ΔLoop
g(r)
r(O_wat-O) (A°)
S134
K292
90°
(D)
K292 (A)
K292 (B)
K292 (C)
r(O_wat-NZ) (A°)

Fig. 8